# Microbial healing of nature-like rough sandstone fractures for rock weathering mitigation

**Zhi-Hao Dong**
Nanjing University
**Xiaohua Pan** ( panxiaohua@nju.edu.cn )
Nanjing University
**Chao-Sheng Tang**
Nanjing University
**Bin Shi**
Nanjing University

**Research Article**

**Keywords:** Sandstone, Weathering fractures, MICP, Bio-healing, Fracture transmissivity, Weathering mitigation

**Posted Date:** January 12th, 2022

**DOI:** https://doi.org/10.21203/rs.3.rs-1197742/v1

# Abstract

Rock weathering fractures in nature are complex and fracture healing is an effective strategy for rock weathering mitigation. This study is a first attempt to apply microbially induced calcium carbonate precipitation (MICP) technology in the healing of nature-weathering-like rough fractures (NWLRF). Sandstone was studied as an example due to it is a wide-spread construction, sculpture and monuments material all over the world. In order to achieve a high healing efficiency, a repeated mixture injection strategy was proposed. Based on a series of laboratory MICP injection experiments on four types of NWLRF, we systematically explored the fundamental micro-healing mechanism and the influence of factors including fracture aperture, characteristics of branch fractures, and cementation solution concentration. Experimental results demonstrated that MICP healing with the repeated mixture injection strategy had the ability to efficiently heal the penetrated NWLRF well with length in centimeter-scale and aperture in millimeter-scale, but cannot heal the non-penetrated branch fractures under low injection pressure. The repeated mixture injection strategy furtherly achieved a high apparent fracture healing ratio and a significant reduction of transmissivity. The apparent fracture healing ratios of all main fractures were higher than 80% and the maximum was 99.1%. Fracture transmissivity was reduced by at least three orders of magnitude from about $1\times10^{-4}$ $m^2/s$ to less than $1\times10^{-7}$ $m^2/s$, and the highest reduction reached to four orders. For the aspect of the effects, larger cementation solution concentration, finer aperture and the existing of penetrated branch fracture were beneficial to improve the healing effect. Moreover, the MICP healing mechanism with high fracture healing ratio and significant reduction of transmissivity on sandstone NWLRF was also analyzed. The research results have important theoretical significance and technical guidance value for the disaster prevention and mitigation of rock weathering.


# Introduction

Rock weathering is a common geological hazard. It often destroys stone cultural relics and geological remains, and affects the stability of rock slopes. Rock fracture is regarded as the first way for rainwater to infiltrate into the rock, and is considered as the dominant effect in accelerating weathering process through freeze-thaw cycles, chemical and biological erosions, etc. (Mckay et al. 2009; Sel and Binal, 2021).

Several researchers had pointed out that permeability reduction in term of fracture healing was an useful strategy for weathering mitigation, and developed various types of chemical healing materials (Cardiano et al. 2005; Guo et al. 2009). Classified by chemical composition, chemical healing materials can be divided into inorganic materials and organic materials. However, both the two types of healing materials are not always preferable in site applications because there are some disadvantages. For example, inorganic materials with large particles such as Portland cement have low permeability and thus are difficult to be penetrated into microfractures, other inorganic materials with low viscosity normally cannot form effective bonding strength among fractures, and organic materials usually have poor weather resistance and durability (Naeimi and Haddad 2020). It thus important to propose a new method with low

viscosity, high bonding strength, good weather resistance and durability, and carbon emission and eco-friendly.

Since the discovery that microbially induced calcium carbonate precipitation (MICP) can be applied for the improvement of soil foundation as a novel, green, effective, and sustainable microbial geotechnical engineering technology ( Ivanov and Chu 2008; DeJong et al. 2010; Van Paassen et al. 2010), a small number of researchers have attempted to verify the feasibility of healing rock fractures using MICP technology, and to explore the hydraulic and mechanical performance. According to the literature review, these researches can be divided in to three scales including small-scale, borehole-scale, and field scale.

For the small-scale conditions, a series of planar flow experiments were carried out on varying single smooth artificial fractures by etching the fractures using transparent rock-like materials or rock materials (Phillips et al. 2013; El Mountassir et al. 2014; Minto et al. 2016). Borehole-scale experiments were mainly radial flow experiments conducted on single artificial rock fractures those were constructed by hydraulic fracturing or saw cutting (Phillips et al. 2013; Minto et al. 2016). Moreover, after Cuthbert et al. (2013) presented a first field experiment applying MICP to reduce a single dacite fracture permeability approximately 25 m below ground level, a few researchers, i.e., Cunningham et al. (2014), Phillips et al. (2016 and 2018), and Kirkland et al. (2020) furthly performed MICP field healing experiments on subsurface single fractures near wellbores for wellbore integrity purpose.

In these studies, all researchers adopted a similar injection strategy namely repeated bacterial injection strategy to ensure an even calcium carbonate precipitation. The repeated bacterial injection strategy means that injecting bacteria solution (BS) first, followed by the cementation solution (CS, $Ca^{2+}$and urea), and the injection process was repeated several cycles until the experiment was completed. The three scales of experiments demonstrated that MICP technology accompanied with a reasonable injection strategy had shown great potential to heal single smooth rock fractures in small-laboratory-scale and to reduce hydraulic properties of single rock fractures in large-field-scale. Micro-structure analysis on small-laboratory-scale experiments also showed that for the horizontal single smooth fractures, gradual reduction in fracture apertures due to calcium carbonate precipitation was the main healing mechanism. It was influenced by hydrodynamics (i.e., velocity, flow rate, and aperture) and the properties of the bacteria solution and the cementation solution. Although researchers would like to design a good injection strategy to precipitate calcium carbonate evenly, it's actually difficult. Ultimately, the precipitated calcium carbonates reduced each fracture to a number of smaller tortuous pathways along the upper and lower fracture surfaces. Part of the $CaCO_3$ crystals, especially at the locations near inlet port bridged across the fracture aperture and formed a hydraulic barrier, resulting in a significant reduction in the hydraulic conductivity.

However, shallow ground weathering fractures in nature have more complex geometric characteristics than these studied smooth single fissures, such as varying surface roughness, abrupt changes in aperture, existing branches, shallow developmental depth. To date, there is limited information related to the MICP healing performance on shallow ground weathering fractures in nature, the feasibility and the

underlying healing mechanism remain poorly understood, which are essential criteria to be investigated for weathering mitigation.

Sandstone is a wide-spread construction, sculpture and monuments material all over the world. These sandstone construction, sculpture and monuments are facing serious weathering hazard, and weathering fracturing is one of the important diseases (Turkington et al. 2005). It is thus necessary and urgent to study the healing problem of sandstone weathering fractures.

Therefore, this study took sandstone as an example, and was a first attempt to investigate the hydraulic performance of adopting MICP to heal nature-weathering-like rough fractures (NWLRF) and to reveal the corresponding micro-healing mechanism. A repeated mixture injection strategy (detailed information can be found in Section of injection strategy) was proposed and a series of laboratory MICP injection experiments were carried out on four types of NWLRF including single fractures with broad aperture, single fractures with fine aperture and multiple fractures with penetrated branch fracture and non-penetrated branch fracture. Accompanied with the conducted relevant observational analysis and hydraulic tests, the spatial distribution of the calcium carbonate precipitation, apparent fracture healing ratio and fracture transmissivity reduction were evaluated, which are key aspects controlling the effect of rock weathering mitigation. In addition, fracture healing mechanism, morphology features of calcium carbonate and effects of fracture aperture, CS concentration and branch fracture were discussed. The research results have important theoretical significance and technical guidance value for the disaster prevention and mitigation of rock weathering.

## Materials And Methodologies

# Materials

The sandstone used in this study was a type of fine green sandstone with grain size varies from 0.2 to 0.5 mm. It was collected from Longchang, Sichuan province, China. The mineral composition of the sandstone was 62% quartz, 18% feldspar, 16% kaolinite, and 4% mica. The density was 2.23 g/cm$^3$ and P-wave velocity was 2.6 km/s. There were no distinct layering or laminations observed from the collected sandstone block.

*Sporosarcina pasteurii* (ATCC 11859), a type of bacteria which can efficiently produce urease and has high urea hydrolysis performance, was used as urease-producing bacteria in this study (Cheng et al. 2020; Liu et al. 2020a). It was cultivated in a sterilized liquid medium consisting of 15.73 g/L Tris base, 10 g/L ammonium sulfate and 20 g/L yeast extract for 24h at 30°C. The optical density ($OD_{600}$) of the collected bacterial culture varied between 1 and 1.2, and the urease activity was 1.1 mM hydrolyzed urea/min.

CS is a mixture of equimolar $Ca^{2+}$ and urea, and a small amount of nutrient broth (3 g/L). In this study, two types of CS concentration including 0.1 M and 0.5 M were adopted to investigate the influence of the

CS concentration on the MICP healing process and the spatial distribution of the calcium carbonate.

# Sample preparation

Mckay et al. (2009) pointed out that thermal stress caused by rapid temperature variations was an important source of rock weathering at the arid area due to the differences in physical and mechanical properties of the rock component minerals. In wet areas, thermal stress played a dominant role in the initial stage of the rock weathering fracture development, and other types of physical and chemical weathering effects such as freeze-thaw cycles and chemical erosion were also involved in the later stage. Thus, cyclic thermal shock processing method which was widely used to generate new random and rough cracks rapidly was adopted to accelerate the physical weathering of sandstone and to prepare the NWLRF in this study (Bruel 2002; Dong et al. 2019). The schematic diagram of sample preparation process including three steps is shown in Fig. 1.

Firstly, three standard size cylindrical sandstone samples were cored from a same sandstone mass, they were 5 cm in diameter and 10 cm in height. Secondly, samples were heated in a high-temperature furnace at 600°C for 1 h, and then were moved to 20°C water for rapid cooling. The cyclic thermal shock processing process was repeated until 1mm aperture fracture appeared on sample surface. Thirdly, the standard size samples with various of NWLRF was cut into small size sub-samples with a thickness of 1 cm along length direction. Samples contained single fracture with broad aperture, single fracture with fine aperture, and multiple fractures with branch fractures were selected as the typical experimental samples. In order to consider both penetrated branch fracture and non-penetrated branch fracture conditions, two branch fractures in one of the multiple fracture sample (M1) were both sealed and one branch fracture was sealed and the other one was not sealed in another multiple fracture sample (M2). The sealed locations can be found in Fig. 1 marked with red points.

Finally, four types of sandstone samples with NWLRF were prepared to simulate the typical shallow ground weathered sandstone in nature because of the thermal stress. Each type of samples was prepared in duplicate (see Fig. 1). The physical dimension of the samples was 5 cm in diameter and 1.0 cm in height. According to the theory of fracture roughness (Barton and Choubey 1977), the fracture roughness coefficients (JRC) of the all the samples were about 18~20. Typical samples of each type were shown in Fig. 1 as examples.

# Injection strategy

The performance and efficiency of fracture healing are mainly controlled by the injection strategy. For different situations and requirements, we need to choose a reasonable injection strategy. It is well known that weathering fractures in nature not only have more complex geometric characteristics than these studied smooth single fissures but also have more numbers on the shallow surface of the weathered rock mass. This requires that the injection strategy proposed for weathering fractures should have high healing efficiency.

Tobler et al. (2018) pointed out that healing efficiency was a major challenge for the widely used repeated bacterial injection strategy. When it was applied to heal single smooth fractures, healing time often took a few days or even a dozen days. The reasons can be explained that bacteria were difficult to fix on the smooth fractures firmly, and most of the bacteria were washed away during the subsequent injection of the CS. Thus, only a small number of bacteria remained on the fracture surface, resulting in a very slow precipitation of calcium carbonate. Moreover, during the repeated bacterial injection process, the precipitation rate of calcium carbonate near the inlet area was slightly higher than other areas. This phenomenon might be more significant in the healing process of weathering fractures due to the varying surface roughness and abrupt changes in aperture. The precipitated calcium carbonate will initially block the fractures near the inlet area with smallest aperture. Other fractures far away from the inlet area are thus not filled well enough to form an effective hydraulic barrier.

Therefore, a repeated mixture injection strategy was adopted in this study for the high healing efficiency purpose. The repeated mixture injection strategy means that BS and CS solutions were mixed in equal volume, and half hour static period was conducted before injection. Ever one knows that when BS and CS solutions are mixed prior to injection, calcium carbonate precipitation begins almost immediately in the mixture, leading to clogging of the inlet ports. The half hour static period was conducted for the adequate deposition of the rapidly formed $CaCO_3$ crystals. The clean supernatant was used as the bio-cement solution for injection.

In order to reduce the effect of sample thickness, the (main) fractures remained vertical during injection process. The upper fractures were the solution inlet and the lower factures were the outlet as shown in Fig. 1. Prior to injection, samples surfaces were covered with soft silicone film and acrylic glass plate, and were clamped with clamps to prevent surface leakage. In this study, 0.5 L BS and 0.5 L CS were used for each sample to ensure sufficient clean supernatant to completely heal each fracture. Previous study demonstrated that MICP can successfully be used to grout a fracture under constantly flowing conditions (Minto et al. 2016). Thus, a constant flow rate of 20 ml/min was adopted to inject the supernatant under a room temperature of 30 ℃ until substantial clogging occurred.

# Characterization of fracture healing performance

Healing performance on NWLRF is evaluated from four aspects including calcium carbonate distribution, morphology features of calcium carbonate on fracture surfaces and across the fracture aperture, apparent fracture healing ratio, and the changes of fracture transmissivity before and after MICP healing.

Fracture surface calcium carbonate distributions were directly observed by microscope and were verified by the internal calcium carbonate distributions through opening the fracture.

The morphology features of calcium carbonate on fracture surfaces and across the fracture aperture were characterized by microscope photos.

Due to the complex geometric characteristics of the NWLRF, quantitative and accurate determination of the whole fracture healing ratio is very difficult. As the (main) fractures remained vertical during injection

process and the effect of sample thickness was reduced, we assumed that the precipitation of calcium carbonate was approximate in the direction of thickness. Thus, apparent fracture healing ratio was used in this study to evaluate the healing performance. Apparent fracture healing ratio was defined as the percent surface fracture space filled by $CaCO_3$ crystals after healing. The apparent fracture healing ratio was estimated by area measurements from the microscope photos using a “Crack Image Analysis System” (CIAS). CIAS developed in previous studies was used to quantify the fracture parameters including length, aperture and area with a calculation accuracy of 0.01mm (Tang et al. 2010).

Fracture transmissivity ($T$, $m^2/s$) describes the ability for fluid flow within the plane of the rock fracture and is defined as the in-plane permeability multiplied by the fracture thickness. $T$ was determined in term of fracture transmissivity test with constant water head in this study. Constant head was adopted because the main source of water that causes weathering is rainfall, osmotic pressure tends to be relatively small. Thus, a small constant head pressure of 3.5 kPa was adopted for the fracture transmissivity test. Prior to the testing, samples were immersed in water for 24 hours to achieve saturation situation, reducing the impact of initial water content on the measurement results. In this study, cubic law was used to determine the $T$. Cubic law was widely used for laminar flow in fractures which was also called parallel plate model (Brown 1987). Normally, flow rate ($Q$, $m^3/s$) can be calculated by Eq. (1), and $T$ can be calculated by Eq. (2) (Witherspoon et al. 1980). Substitute Eq. (1) into Eq. (2), $T$ can be calculated by $Q$, $L$, $\Delta h$, and $W$ as shown in Eq. (3).

$$Q = \frac{W}{L}\left(\frac{\rho g}{12\mu}\right)b_h^3 \Delta h \quad (1)$$

$$T = \left(\frac{\rho g}{12\mu}\right)b_h^3 \quad (2)$$

$$T = \frac{QL}{\Delta h W} \quad (3)$$

where $L$ is the fracture length (m), $W$ is the width in the direction normal to fluid flow (m), $\rho$ is fluid density ($kg/m^3$), $g$ is acceleration due to gravity ($m/s^2$), $\mu$ is fluid dynamic viscosity (kg/(ms)), $\Delta h$ the head loss (m), $V$ is fluid velocity (m/s), and $b_h$ is hydraulic aperture (m).

# Results

# Distribution of calcium carbonate

After MICP healing, apparent distribution of white calcium carbonate on fracture surface was clearly observed as shown in Fig. 2(a). Fig. 2a shows that precipitated calcium carbonates filled all the fractures well except non-penetrated branch fractures of multiple fracture samples M-1 and M-2. For the non-penetrated branch fractures, only small amounts of calcium carbonates were observed near the main

fractures. This indicates that MICP technology can heal penetrated rough weathering main and branch fractures well with length in centimeter-scale and aperture in millimeter-scale, but cannot heal the non-penetrated branch fractures with low injection pressure. The apparent distribution of calcium carbonate of each sample was verified by the internal calcium carbonate distributions as shown in Fig. 2b.

# Morphology features of calcium carbonate

We can observe from the microscope photos of overall surface fractures (Fig. 3a) that the macro-healing features of the precipitated calcium carbonate in main fractures and penetrated branch fractures were dense and stable after transmissivity test subjected to constant water head. Meanwhile, it is important to note that multi shapes, various sizes, and different depths of un-healed fractures are distributed within the calcium carbonate fillings along the fractures. For examples, the shallow un-healed fracture (indicated by the white dotted oval in Fig. 3a) and deep un-healed fracture (indicated by the red dotted oval in Fig. 3a) are the two typical types. The comparison of each subgraph indicates that there were more un-healed fractures, especially the deep un-healed fractures in the samples with broad aperture and healed with low CS concentration solution, i.e., B-1 and M-1. Moreover, small amounts of loose calcium carbonate can be observed in the non-penetrated branch fractures. The difference of the macro-healing features was induced by the varying micro-morphology features.

To have a better understanding of the micro-morphology features of the precipitated calcium carbonates at different locations, some typical microscope photos of calcium carbonates at fully filled area, un-healed fracture area and non-penetrated branch area were presented on Fig. 3b. Calcium carbonates at fully filled area were dense and had great number of small voids among them (Fig. 3b-1). These dense calcium carbonates consisted of small round $CaCO_3$ crystals and bonded firmly with each other together, completely filling the fracture aperture and bridging across the both fracture surfaces. This type of micro-morphology feature was most existed on samples B-2, F-2, F-2 and M-2. Calcium carbonates at shallow un-healed fracture area also consisted of small round $CaCO_3$ crystals with a rough surface, and looked slightly looser than that at fully filled area (Fig. 3b-2). For deep un-healed fracture, calcium carbonates were distributed in cluster on both fracture surfaces and looked much looser than those at fully filled area and at shallow un-healed fracture area (Fig.3b-3). These two types of micro-morphology features at un-healed fracture area were most existed on samples B-1 and M-1. At non-penetrated branch area of samples M-1 and M-2, a small number of granular calcium carbonates were absorbed on both fracture surfaces (Fig. 3b-4).

The macro-healing features of the precipitated calcium carbonate internal the fractures were also investigated by microscopic observation. Typical microscope photos were showed on Fig. 3c. Compared to fracture surface, same phenomenon internal the fractures that a lot of small voids at fully filled area (Fig. 3c-1) and sparse granular calcium carbonates at non-penetrated branch area (Fig. 3c-4) was also observed. Meanwhile, round bubble-like voids (Fig. 3c-2) and long bubble-like voids (Fig.3c-3) were discovered internal the fracture. The surfaces of both types of bubble-like voids were smooth, which were the main difference from those of un-healed fracture surface.

# Apparent fracture healing ratio

Grayscale images of samples before and after MICP healing are showed in Fig. 4. Fig. 4 indicates that all the fracture area significantly reduced except non-penetrated branch fractures of multiple fracture samples M-1 and M-2. The detail information of fracture area of samples before and after MICP healing can be found in Fig. 5a and 5b.

The apparent fracture healing ratios (Fig. 5c) of all main fractures are higher than 80% and larger CS concentration (0.5M) healed samples have slightly higher apparent fracture healing ratios than those samples healed with 0.1M CS. When the CS concentration is the same, apparent fracture healing ratios of samples with fine aperture fracture are slightly greater than those samples with broad aperture fracture. Thus, for single fracture, fracture healing ratio of sample N-2 with fine aperture fracture and healed by 0.1M CS reaches to 87.7%. For multiple fractures, the existing of penetrated branch fracture promoted the performance of healing. For example, the apparent fracture healing ratios of main fracture and other two non-penetrated branch fractures of sample M-1 are 83.6%, 15.4%, and 41.3%, respectively, while the apparent fracture healing ratios of main fracture and other non-penetrated and penetrated branch fractures of sample M-2 increased to 96.3%, 60.9%, and 99.1%, respectively.

Compared to previous healed results using the repeated bacteria injection strategy which had about 67% facture healing ratio (Tobler et al. 2018), the repeated mixture injection strategy had better healing performance.

# Fracture transmissivity

Fracture transmissivities of various samples before and after MICP healing are showed in Fig. 6. Before MICP healing, fracture transmissivities of all samples close to the order of $10^{-4}$ $m^2/s$ and samples with fine aperture fracture have slight lower values. After the MICP healing, the fracture transmissivity decreased by at least three orders of magnitude from about $1\times10^{-4}$ $m^2/s$ to less than $1\times10^{-7}$ $m^2/s$, and the maximum reduction reaches to four orders of sample F-2 (Fig. 6). For the same aperture, the fracture transmissivity of samples healed by 0.5 M CS (samples B-2, F-2, and M-2) were about 2~3 times higher than those healed by 0.1 M CS (samples B-1, F-1, and M-1), indicating that the 0.5 M CS has better healing performance on NWLRF in this study conditions. This is in consist with the results of apparent fracture healing ratios that samples healed with 0.5 M CS have higher apparent fracture healing ratios and more dense calcium carbonate precipitation.

## Discussions

# Fracture healing mechanism

The schematic diagram of the MICP healing mechanism on NWLRF is shown in Fig. 7. It consists of three main steps.

In the initial stage of injection, bacteria in bio-cement solution were fixed to the both fracture surfaces through two ways. The first way was for the mixture to enter the pores in the fracture surface. Another way was for bacteria to adsorb directly on the fracture surfaces. Due to the rough fracture surface and abrupt changes in aperture, the adsorbed bacteria were unevenly distributed along the length of the fracture. The reason was the fact that solution flow rate in different locations were different (Mountassir et al. 2014). As shown in Fig. 7a, at the convex, the flow rate slowed down, thus more bacteria were adsorbed than other locations. Because of using the repeated mixture injection strategy, the existing of the CS fixed the bacteria firmly to the pores or the fracture surfaces in term of the followed calcium carbonate precipitation.

The second step was the homogeneous precipitation process of calcium carbonate. After the fixing of the bacteria, the repeated mixture injection strategy accelerated the precipitation rate of calcium carbonate on the fracture surfaces than that using repeated bacteria injection strategy. Especially at the convex, calcium carbonate precipitation was relatively faster because there were more bacteria (see Fig. 7b). As more calcium carbonates were precipitated at the convex, more bacteria were furtherly fixed to these $CaCO_3$ crystals. This mutually promoting process finally induced a homogeneous precipitation of calcium carbonate along the fracture length and formed many narrow necks (see Fig. 7b).

The third step was the $CaCO_3$ crystal clogging process and further bonding process among the clogged $CaCO_3$ crystals. Although the clean supernatant was used as the bio-cement solution for injection, abundant of small size $CaCO_3$ crystals (a few microns to tens of microns) were still formed in the bio-cement solution during healing process. When the smallest fracture apertures at narrow necks were reduced to a few tens of microns, these $CaCO_3$ crystals formed in the bio-cement solution clogged the necks immediately. Soon afterwards, more pre-existing $CaCO_3$ crystals partly filled the un-healed fractures quickly. It agreed with previous study (Saada et al. 2006) which pointed out that a solution was able to penetrate pore space if the pore space size was 1.5–2.5 times greater than that of the largest solid particle of the solution. At this time, these fast-filling calcium carbonates were still loose accompanied with multi shapes, various sizes, and different depths of un-healed fractures as shown in Fig. 7c. The large pore space and discontinued un-healed fractures allowed clean bio-cement solutions still to be injected into the fractures. These bio-cement solutions precipitated more $CaCO_3$ crystals among those fast-filling calcium carbonates, and on un-healed fracture surfaces. As a result, fast-filling calcium carbonates were firmly bonded with each other and completely closed up the fracture, providing a stable hydraulic barrier.

The formation of bubble-like voids was accepted to be related to the presence of gas bubbles due to their smooth surface. The gas might come from the air mixed during the injection process (Tobler et al. 2018). On the other hand, the gas might be related to the biogas produced by bacterial activity. Biogas was a type of gas produced through microbial reactions under certain conditions, such as carbon dioxide ($CO_2$) and nitrogen ($N_2$) gas (He et al. 2014; Rebata-Landa and Santamarina 2012). It was believed that the hydrolysis of urea by bacteria produced carbon dioxide ($CO_2$) and ammonia gas ($NH_3$), which were not all

involved in the formation of calcium carbonate or dissolved in water, and the undissolved part formed gas bubbles inside the fractures (see Fig. 7b). When gas bubbles appeared, calcium carbonates precipitated around them, eventually forming round bubble-like voids. In some cases, some small gas bubbles merged into large and long bubbles, thus forming long bubble-like voids (see Fig. 7c).

# Effect of fracture aperture

The fracture aperture influences on the healing performance of MICP. Single fractures with fine aperture have a higher apparent fracture healing ratio than that of single fractures with broad aperture. The reasons can be explained as follows. Healing single fractures with broad aperture requires more precipitated calcium carbonate to fully fill the fracture, which means more healing cycles are needed. This is consistent with the observation that the injection time for single fractures with broad aperture were longer. As mentioned above, the precipitation rate of calcium carbonate was different at different locations. The longer the injection time, the more heterogeneous the precipitated calcium carbonates. Thus, there were more formed narrow necks. These narrow necks could easily cause clogging, generating multi shapes, various sizes, and different depths of un-healed fractures. On the other hand, flow rate in fine fracture was larger, ensuring that bacteria were more evenly distributed along the fracture surface. This reduced the likelihood of the forming of the narrow necks. Therefore, these two aspects resulted in higher apparent fracture healing ratio and lower fracture transmissivity of single fractures with fine aperture.

# Effect of cementation solution concentration

In general, the larger the CS concentration, the higher the apparent fracture healing ratio and less amount of un-healed fractures. Previous studies suggested that high CS concentration would yield large size of calcium carbonate crystals with high calcium carbonate production rate (Al Qabany et al. 2012). This means that compared to low CS concentration, the healing times were fewer when fractures were healed by high CS concentration. Thus, uneven precipitation of calcium carbonate was reduced. When the smallest fracture apertures at narrow necks were reduced to a few tens of microns, those large size of $CaCO_3$ crystals formed in the bio-cement solution clogged the necks immediately and filled the fractures uniformly. Therefore, samples healed with large CS concentration had higher apparent fracture healing ratio and lower fracture transmissivity.

# Effect of branch fracture

In multiple fractures, during the injection process, the main fracture acted as the dominant flow channel, through which the bio-cement solution was preferred. Experimental results indicated that the existing of penetrated branch fractures could promote the healing performance such as increasing apparent fracture healing ratio and decreasing fracture transmissivity of the main fractures. This is can be explained as the fact that the existing of penetrated branch fractures increased the cross-sectional area of the fractures near outlet. It reduced the flow rate of the bio-cementation at the bottom main fractures and branch fractures, ensuring the bacteria to be more evenly distributed in these areas. On the other hand, after the clogging occurred at the necks, the dis-closed penetrated branch fractures allowed extra clean bio-cement

solutions to be injected in to the fractures, even the main fissure was completely closed. The extra clean bio-cement solutions precipitated more $CaCO_3$ crystals furtherly bonded the fast-filling calcium carbonates more firmly and filled more pore spaces and un-healed fractures. While for the non-penetrated branch fractures, due to the presence of air obstruction, only a small amount of the bio-cement solutions seeped into the non-penetrated branch fractures by capillary force and other actions. Thus, it is difficult to form large amount of calcium carbonate crystals on the non-penetrated branch fractures and slightly affect the healing process of the main fracture.

# Conclusions

Four types of sandstone NWLRF were prepared to simulate the shallow ground sandstone weathered by the thermal stress in nature, including single fractures with broad aperture, single fractures with fine aperture and multiple fractures with penetrated branch fracture and non-penetrated branch fracture. In order to have a high healing efficiency, a repeated mixture injection strategy was proposed. According to the analysis of the testing results of the laboratory MICP injection experiments, the main findings are as follows.

(1) MICP healing with the repeated mixture injection strategy can efficiently heal penetrated NWLRF well with length in centimeter-scale and aperture in millimeter-scale but cannot heal the non-penetrated branch fractures under low injection pressure.

(2) The repeated mixture injection strategy also ensured the apparent fracture healing ratios of all main fractures were higher than 80% and the maximum was 99.1%. It was much larger than that of smooth factures healed with repeated bacteria injection strategy.

(3) The apparent fracture healing ratio was affected by the fracture aperture, CS concentration, and branch fracture. Larger CS concentration (0.5M), finer aperture and existing of penetrated branch fracture can promote the apparent fracture healing ratio.

(3) Fracture transmissivity was reduced by at least three orders of magnitude from about $1\times10^{-4}$ $m^2/s$ to less than $1\times10^{-7}$ $m^2/s$, and the highest reduction reached to four orders.

(4) The MICP healing mechanism of varying healing ratios on sandstone NWLRF can be explained as that calcium carbonates grew at different rates from the both fracture surfaces to the middle in different locations at the initial stage. The grow rate of calcium carbonates at convex was the highest and many narrow necks were formed at these neck locations. Subsequently, $CaCO_3$ crystals pre-formed in the bio-cement solution clogged the necks and filled the fractures immediately. Among the fast-filling calcium carbonates, there might be un-healed fractures with multi shapes, various sizes, and different depths. Finally, clean bio-cement solutions was further injected into the fractures. Fast-filling calcium carbonates were firmly bonded with each other and completely closed up the fracture, providing a stable hydraulic barrier.

# Declarations


### Funding

This work was supported by the National Key Research and Development Program of China (2020YFC1808000), National Natural Science Foundation of China (Grant No. 42007244, 41925012, 41902271, 41772280), and Open Fund of State Key Laboratory of Geohazard Prevention and Geoenvironment Protection (Grant No. SKLGP2021K013).


### Competing Interests

The authors have no relevant financial or non-financial interests to disclose

### Author Contributions

The authors of Xiao-Hua Pan and Chao-Sheng Tang contributed to the study conception and design. Material preparation and data collection were performed by Zhi-Hao Dong. The first draft of the manuscript was written by Zhi-Hao Dong, and was imrpoved by Xiao-Hua Pan, Chao-Sheng Tang and Bin Shi. All authors commented on previous versions of the manuscript. All authors read and approved the final manuscript.

# Acknowledgement


This work was supported by the National Key Research and Development Program of China (2020YFC1808000), National Natural Science Foundation of China (Grant No. 42007244, 41925012, 41902271, 41772280), and Open Fund of State Key Laboratory of Geohazard Prevention and Geoenvironment Protection (Grant No. SKLGP2021K013).


# References


1. Al Qabany A, Soga K, Santamarina C (2012) Factors affecting efficiency of microbially induced calcite precipitation. J Geotech GeoEnviron Eng 138:992–1001
2. Barton N, Choubey V (1977) The shear strength of rock joints in theory and practice. Rock mechanics 10:1–54
3. Brown SR (1987) Fluid flow through rock joints: the effect of surface roughness. Journal of Geophysical Research: Solid Earth 92:1337–1347
4. Bruel D (2002) Impact of induced thermal stresses during circulation tests in an engineered fractured geothermal reservoir, Oil & Gas Science and technology Rev. IFP 57(5):459–470
5. Cardiano P, Ponterio RC, Sergi S, Schiavo SL, Piraino P (2005) Epoxy-silica polymers as stone conservation materials. Polymer 46(6):1857–1864

6. Cheng L, Kobayashi T, Shahin MA (2020) Microbially induced calcite precipitation for production of “bio-bricks” treated at partial saturation condition. Constr Build Mater 231C:117095–117095
7. Cheng L, Shahin MA, Chu J (2019) Soil bio-cementation using a new one-phase low-pH injection method. Acta Geotech 14:615–626
8. Cunningham AB, Phillips AJ, Troyer E, Lauchnor R, Hiebert R, Gerlach R, Spangler LH (2014) Wellbore leakage mitigation using engineered biomineralization. Energy Procedia 63:4612–4619
9. Cuthbert MO, McMillan LA, Handley-Sidhu S, Riley MS, Tobler DJ, Phoenix VR (2013) A field and modeling study of fractured rock permeability reduction using microbially induced calcite precipitation. Environ Sci Technol 47:13637–13643
10. DeJong JT, Mortensen BM, Martinez BC, Nelson DC (2010) Bio-mediated soil improvement. Ecol Eng 36:197–210
11. Dong Z, Sun Q, Ranjith PG (2019) Surface properties of grayish-yellow sandstone after thermal shock. Environ Earth Sci 78:420
12. Mountassir EI, Lunn GE, Moir RJ, MacLachlan H E (2014) Hydrodynamic coupling in microbially mediated fracture mineralization: Formation of self-organized groundwater flow channels. Water Resour Res 50:1–16
13. Guo QL, Wang XD, Zhang HY, Li ZX, Yang SL (2009) Damage and conservation of the high cliff on the Northern area of Dunhuang Mogao Grottoes, China. Landslides 6:89–100
14. He J, Chu J, Ivanov V (2014) Mitigation of liquefaction of saturated sand using biogas. Bio-and Chemo-Mechanical Processes in Geotechnical Engineering: Géotechnique Symposium in Print 2013. ICE Publishing 116-124
15. Ivanov V, Chu J (2008) Applications of microorganisms to geotechnical engineering for bioclogging and biocementation of soil in situ. Reviews in Environmental Science and Bio/Technology 7:139–153
16. Kirkland CM, Thane A, Hiebert R, Hyatt R, Kirksey J, Cunningham AB, Gerlach R, Spangler L, Phillips AJ (2020) Addressing wellbore integrity and thief zone permeability using microbially-induced calcium carbonate precipitation (MICP): A field demonstration. J Petrol Sci Eng 190:107060
17. Liu B, Zhu C, Tang CS, Xie YH, Yin LY, Cheng Q, Shi B (2020a) Bio-remediation of desiccation cracking in clayey soils through microbially induced calcite precipitation (MICP). Eng Geol 264:105389
18. Liu D, Shao A, Jin C, Yang L (2018) Healing technique for rock cracks based on microbiologically induced calcium carbonate mineralization. J Mater Civ Eng 30:04018286
19. Liu S, Yu J, Peng X, Cai Y, Tu B (2020b) Preliminary study on repairing tabia cracks by using microbially induced carbonate precipitation. Constr Build Mater 248:118611
20. Mckay CP, Molaro JL, Marinova MM (2009) High-frequency rock temperature data from hyper-arid desert environments in the Atacama and the Antarctic Dry Valleys and implications for rock weathering. Geomorphology 110(3–4):182–187

21. Minto JM, MacLachlan E, El Mountassir G, Lunn RJ (2016) Rock fracture injection with microbially induced carbonate precipitation. Water Resour Res 52:8827–8844
22. Naeimi M, Haddad A (2020) Environmental impacts of chemical and microbial injection. Environ Sci Pollut Res 27:2264–2272
23. Peng S, Di H, Fan L, Fan W, Qin L (2020) Factors Affecting Permeability Reduction of MICP for Fractured Rock. Frontiers in Earth Science 8:217
24. Phillips AJ (2013) Biofilm-induced calcium carbonate precipitation: application in the subsurface. Montana State University-Bozeman, College of Engineering
25. Phillips AJ, Cunningham AB, Gerlach R, Hiebert R, Hwang C, Lomans BP, Westrich J, Mantilla C, Kirksey J, Esposito R (2016) Fracture sealing with microbially-induced calcium carbonate precipitation: A field study. Environ Sci Technol 50:4111–4117
26. Phillips AJ, Lauchnor E, Eldring J, Esposito R, Mitchell AC, Gerlach R, Cunningham AB, Spangler LH (2013) Potential $CO_2$ leakage reduction through biofilm-induced calcium carbonate precipitation. Environ Sci Technol 47:142–149
27. Phillips AJ, Troyer E, Hiebert R, Kirkland C, Gerlach R, Cunningham AB, Spangler L, Kirksey J, Rowe W, Esposito R (2018) Enhancing wellbore cement integrity with microbially induced calcite precipitation (MICP): a field scale demonstration. J Petrol Sci Eng 171:1141–1148
28. Rebata-Landa V, Santamarina JC (2012) Mechanical effects of biogenic nitrogen gas bubbles in soils. J Geotech GeoEnviron Eng 138:128–137
29. Saada Z, Canou J, Dormieux L, Dupla JC (2006) Evaluation of elementary filtration properties of a cement grout injected in a sand. Can Geotech J 43:1273–1289
30. Sel A, Binal A (2021) Does bacterial weathering play a significant role in rock weathering? Environ Earth Sci 80:778
31. Turkington AV, Paradise TR (2005) Sandstone weathering: a century of research and innovation. Geomorphology 67(1–2):229–253
32. Tang CS, Cui Y, Tang AM, Shi B (2010) Experiment evidence on the temperature dependence of desiccation cracking behavior of clayey soils. Eng Geol 114:261–266
33. Tobler DJ, Minto JM, El Mountassir G, Lunn RJ, Phoenix VR (2018) Microscale analysis of fractured rock sealed with microbially induced CaCO3 precipitation: influence on hydraulic and mechanical performance. Water Resour Res 54:8295–8308
34. Van Paassen LA, Ghose R, van der Linden TJ, van der Star WR, van Loosdrecht MC (2010) Quantifying biomediated ground improvement by ureolysis: large-scale biogrout experiment. J Geotech GeoEnviron Eng 136:1721–1728
35. Witherspoon PA, Wang JS, Iwai K, Gale JE (1980) Validity of cubic law for fluid flow in a deformable rock fracture. Water Resour Res 16:1016–1024

# Tables

Table 1 The length, aperture and area of the fracture of each sample calculated by the CIAS

| Fracture type | Sample notation | Fracture | Length (mm) | Aperture (mm) | Area ($mm^2$) |
|---|---|---|---|---|---|
| Broad aperture single fracture | B-1 | Main fracture | 55.76 | 0.74 | 38.00 |
| | B-2 | Main fracture | 56.21 | 0.71 | 37.06 |
| Fine aperture single fracture | F-1 | Main fracture | 54.77 | 0.41 | 21.17 |
| | F-2 | Main fracture | 59.70 | 0.37 | 20.34 |
| Multiple fracture | M-1 | Main fracture | 60.19 | 0.74 | 44.83 |
| | | Branch fracture 1 | 25.29 | 0.22 | 5.21 |
| | | Branch fracture 2 | 28.40 | 0.27 | 7.06 |
| | M-2 | Main fracture | 57.70 | 0.73 | 43.08 |
| | | Branch fracture 1 | 31.20 | 0.31 | 9.20 |
| | | Branch fracture 2 | 28.69 | 0.38 | 11.21 |
| Note: B-1, F-1, M-1 were treated by 0.1M CS, and B-2, F-2, M-2 were treated by 0.5M CS. | | | | | |

# Figures

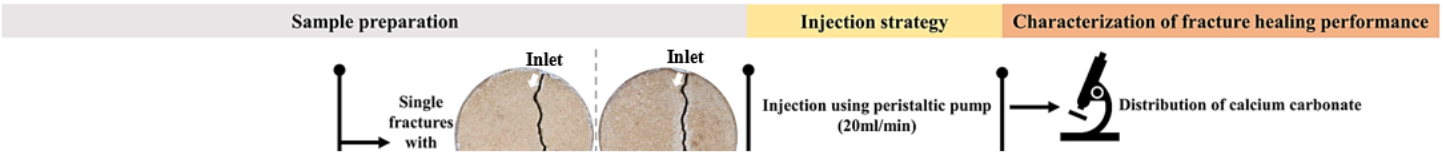


**Figure 1**

Schematic diagram of MICP healing experiment on nature-weathering-like rough fractures including sandstone sample preparation, injection strategy and characterization of fracture healing performance

## Figure 2

Calcium carbonate distribution on (a) fracture surfaces, and (b) internal positions across the fracture aperture

## Figure 3

(a) macro-healing features of the precipitated calcium carbonate on fracture surface of each type of samples, (b) typical microscope photos of precipitated calcium carbonates on fracture surfaces at (1) a fully filled area, (2) a shallow un-healed fracture area, (3) a deep un-healed fracture area, and (4) a non-penetrated branch area, and (c) typical microscope photos of precipitated calcium carbonates internal the fractures with (1) small voids, (2) round bubble-like voids, (3) long bubble-like voids, and (4) spare calcium carbonate distribution

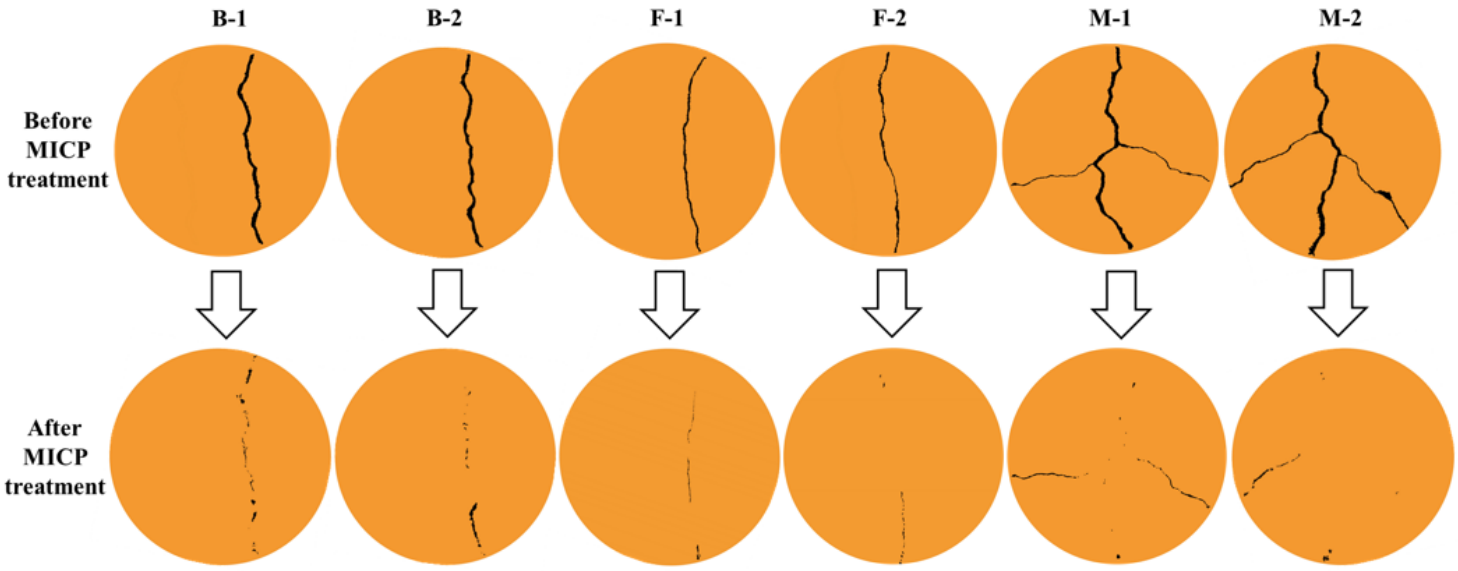


## Figure 4

Grayscale images of samples before and after MICP healing

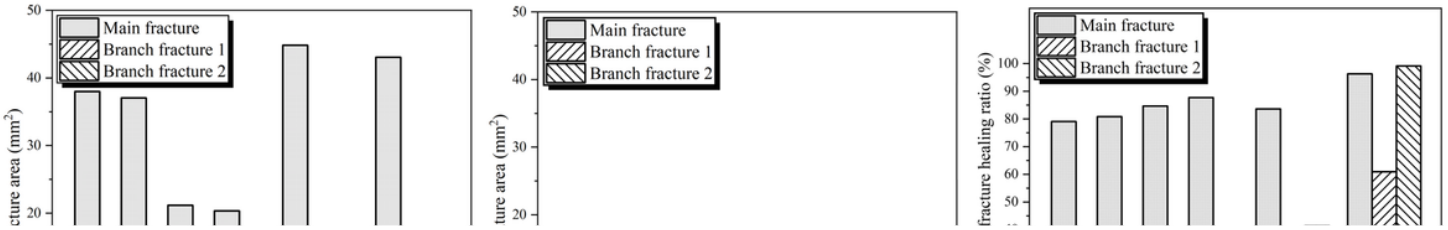


**Figure 5**

Fracture area calculated by Crack Image Analysis System of samples (a) before MICP healing, (b) after MICP healing, and related (c) apparent fracture healing ratio

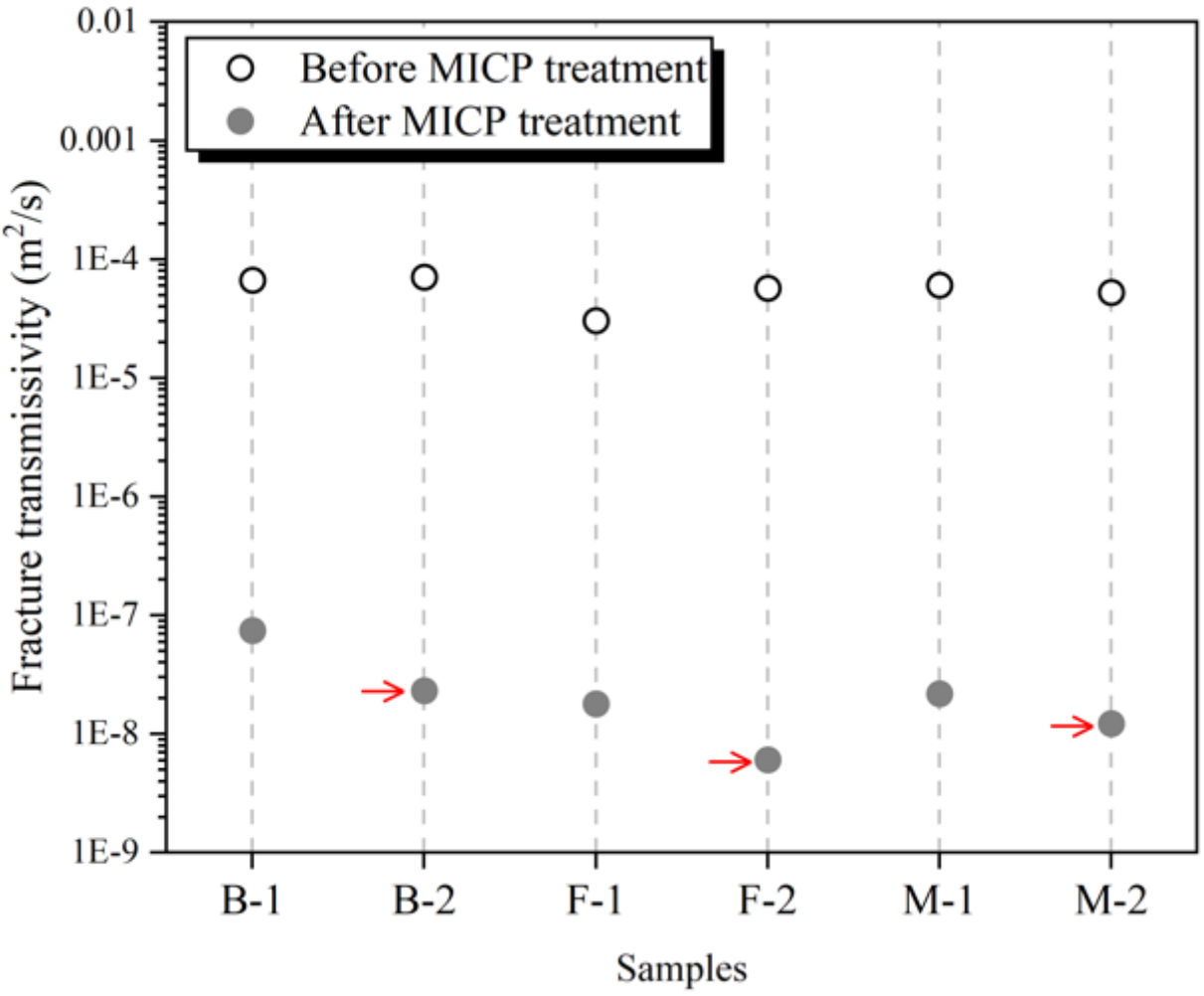


**Figure 6**

Fracture transmissivities of various samples before and after MICP healing

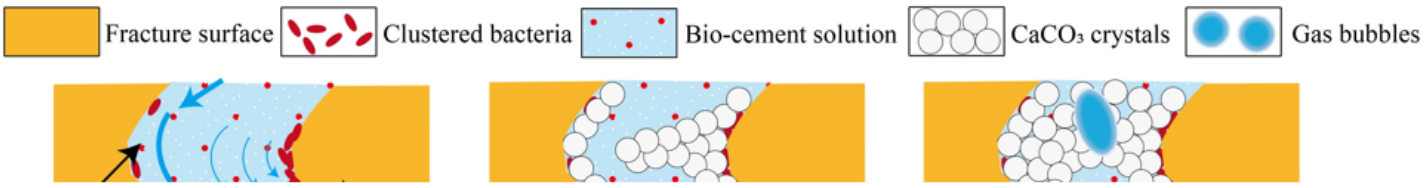


**Figure 7**

The schematic diagram of the MICP healing mechanism on natural-weathering-like rough fractures including three main steps, (a) more bacteria are attached to the convex with low flow rate, (b) formation of narrow necks and gas bubbles, (c) discontinued un-healed fracture area and fully filled area formed along fracture length direction

## Supplementary Files

This is a list of supplementary files associated with this preprint. Click to download.

- Highlights.docx